A Compact 16-Channel Input Thermally Adsorption-/Desorption-Controlled Intelligent Odor Sensing System

Toshiki Niinomi, Atsuo Nakao, Yosuke Hanai, Hiroshi Ushio, Takuya Hayashi, and Masaya Nakatani

***Abstract*—In this study, we developed a compact thermally adsorption-/desorption-controlled odor sensing system (TC-OSS). The absorption and desorption of odor molecules or volatile organic compounds (VOCs) are controlled by sensor temperature giving a high resistance value in a VOC adsorbed state at low temperature and a low resistance in a VOC desorbed state at a high temperature. The system eliminates many gas flow control parts required in conventional odor sensing systems realizing a significant compactness. The developed TC-OSS comprises a 16-channel VOC sensing elements array fabricated on a small heater showing high sensitivity (3-ppb sensing capability with signal-to-noise ratio (SNR) as high as ∼15 dB). With the assistance of artificial intelligence (AI) postprocessing, a discriminative classifier of five standard VOCs with high a successful probability (∼95.8%) is demonstrated.**

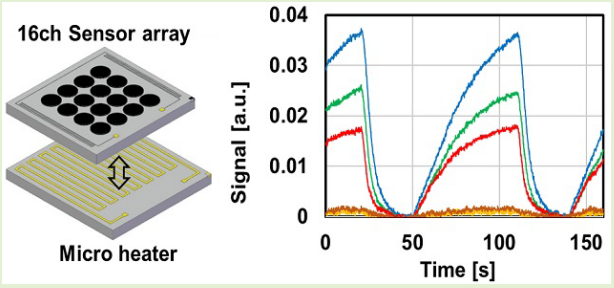

***Index Terms*— Discriminative classifier, fluidly adsorption-/desorption-controlled Odor sensing system (FC-OSS), polymer-nanocomposite conductive membrane (PCM), Principal component analysis (PCA), thermally adsorption-/desorption-controlled odor sensing system (TC-OSS), volatile organic compounds (VOCs).**

I. Introduction

THE odor sensing systems (OSSs) capable of identifying odor molecules similar to human and animal olfactory receptors are highly expected for applications to hygiene management [1], environmental monitoring [2], medicines [3], [4], individual authentication [5], prevention of fire disasters [6], and food industry [7]. A practical OSS must be equipped with two functionalities; a high sensitivity to odor molecules or volatile organic compounds (VOCs) contained in air with tiny fractional amounts (typically with ppm or lower order) and a capability of identifying or discriminating various VOCs. To meet these requirements, in recent years, arrayed OSSs powered by machine learning or artificial intelligence (AI) systems are intensively developed [8], [9], [10], [11], [12].

A common architecture of such an OSS consists of: 1) an integrated arrayed sensor chip with several to several hundred types of VOC-sensing materials that respond differently to different VOCs; 2) a module that pattern-recognizes sensor responses using statistical methods such as principal component analysis (PCA) [13] and AI based on a deep-learning system [14]; 3) an inlet/outlet gas-flow control system consisting of a flow path that connects the input line for VOCs (and a reference gas) to a main chamber containing the sensor module and to the outlet from which the used gas is pumped; and 4) a system that controls adsorption and desorption of odor molecules impinging on the sensing devices. Regarding to 1), various types of chemical sensors have been proposed. Sensors utilizing a MOSFET [15], a quartz crystal microbalance (QCM) [16], and surface acoustic wave (SAW) filters [17] as transducers, have been developed. We have been developing sensors using carbon nanoparticles [1], [18], [19] as transducers because of their high sensitivities. Regarding to 4), in conventional OSSs, desorption of VOCs is done simply by exposing the sensing elements to a clean (or filtered) gas or pure nitrogen introduced from an inlet line "independent of" a sample gas line for a sufficiently long period as illustrated in Fig. 1(b). Such systems require not only a filter for the reference gas but also an electrically controlled valve for switching the flow of the VOCs. Although such systems have been demonstrated their high level of utility [1], [18], [19], downsizing the entire system is difficult because of the existence of the flow control system with many parts. For practical applications where OSSs are set in a car and on

Manuscript received 1 December 2023; accepted 30 January 2024. Date of publication 8 February 2024; date of current version 2 April 2024. The associate editor coordinating the review of this article and approving it for publication was Prof. Minhee Yun. *(Corresponding author: Toshiki Niinomi.)*

The authors are with Panasonic Industry Corporation, Kadoma, Osaka 571-8501, Japan (e-mail: niinomi.toshiki@jp.panasonic.com).

Digital Object Identifier 10.1109/JSEN.2024.3361855

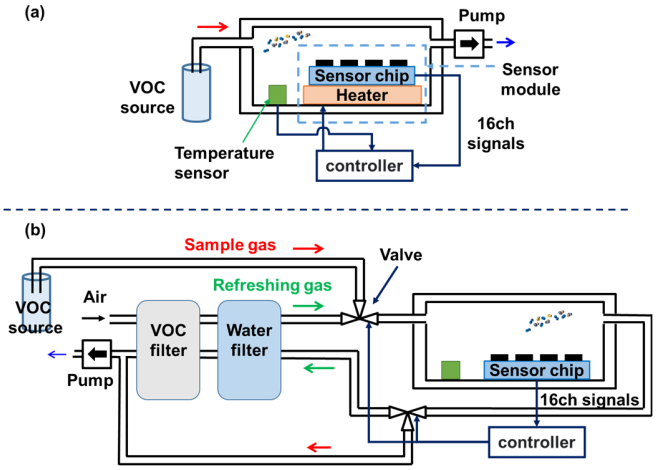

Fig. 1. Architecture of (a) TC-OSS and (b) FC-OSS. TC-OSS does not require an input fluidic system.

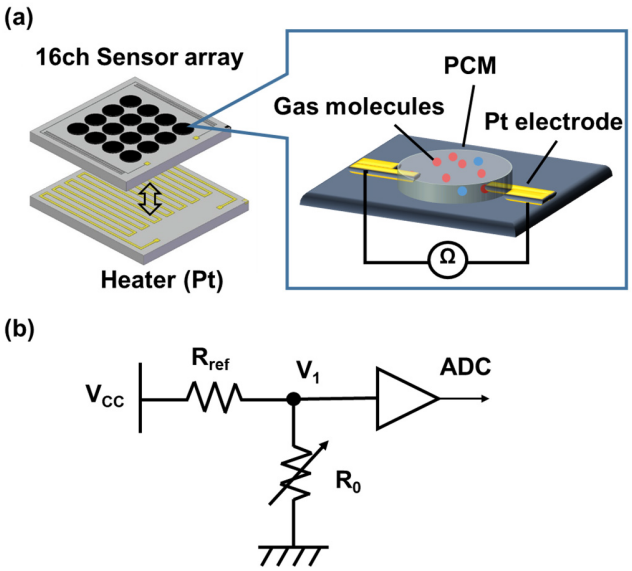

Fig. 2. (a) Chemical sensor for detection of gas molecules and (b) voltage divider for resistance measurements.

a drone [20], a robotics system [21], downsizing is essential. The systems are also considered to be applicable to specific social infrastructures such as wastewater/garbage treatment plants [20], plant pest and disease monitoring sites [22], and composting plants [23].

In this article, in order to downsize a conventional OSS, we propose a new OSS in which the adsorption and desorption of VOCs are thermally controlled. The new control system not only eliminates the many flow-control parts but also makes the reset operation independent of the input flow-control operation. The conventional system requires a water filter and a VOC filter to generate refreshing gas, and valves to switch between refreshing gas and sample gas from the VOC source, but the new system does not use refreshing gas, so these parts are not required. The newly developed OSS is equipped with a 16-channel-chemical sensor array composed of heat-resistant materials, with a small heater and with a postprocessor of an AI software. A high sensitivity to VOCs [down to ppb level with 15-dB signal-to-noise ratio (SNR)] and high capability of discriminative classification of standard test VOCs (with a typical success rate of 95.8%) are demonstrated.

II. Systems and Materials

A. Thermally Adsorption-/Desorption-Controlled Odor Sensing System

In Fig. 1(a), the configuration of the presently developed thermally adsorption-/desorption-controlled OSS (TC-OSS) is shown. The TC-OSS consists of an odor sensing elements (OSELs) array, of a heater underneath the OSEL array, of a data processing system including a controller and a postprocessor with an AI function. The temperature of the OSEL array is raised to desorb VOCs and lowered to adsorb VOCs simply by turning on and off the heater, respectively. The temperature control system comprises a feedback loop with a temperature sensor, a controller, and a heater.

During operation, the TC-OSS is set in a chamber where VOCs diluted in a reference gas are introduced from an inlet system. It is emphasized that this configuration is significantly smaller and simpler than that of a conventional fluidly adsorption-/desorption-controlled OSS (FC-OSS), as illustrated in Fig. 1(b). In addition to the main sensing module, in an FC-OSS, at least two independent source gas lines connected after an inlet control valve, two filters for producing a refresh gas, and direct and filtered exhaustion gas lines controlled by an outlet valve are required. Furthermore, mutual dependence on controlling the gas flow and sensor status (adsorption/desorption) is considered to be a serious disadvantage for practical applications. Thus, the configuration of the FC-OSS suffers from inherent complexity in system implementation and architecture [1], [19].

B. Odor Sensing Element

In Fig. 2(a), a schematic of the developed 16-channel OSEL array is illustrated. Each OSEL consists of a polymer-nanocomposite conductive membrane (PCM) dispersed with carbon nanoparticles exhibiting a finite resistance (R_O) [1]. On adsorbing VOC molecules, the PCM expands in volume and exhibits a higher resistance ($R_{O,a}$) than that before the adsorption ($R_{O,b}$) showing VOC sensitivity. For quantification, a sensitivity parameter, Sen, (defined as follows) is used:

$$\text{Sen} = \frac{R_{O,a} - R_{O,b}}{R_{O,b}}. \tag{1}$$

To obtain R_O ($R_{O,a}$ and $R_{O,b}$), we measure a voltage across R_O denoted by V_1, in series with a reference resistor, R_{ref}, under a constant bias voltage denoted by V_{CC} [Fig. 2(b)]. With this configuration, R_O at any status of an OSEL is calculated as follows:

$$R_O = \frac{V_1}{V_{cc} - V_1} \cdot R_{\text{ref}}. \tag{2}$$

On the other hand, the selection of PCM materials is based on two criteria. First, to sense a variety of VOCs, the range of the McReynolds constants [24] of 16 PCMs is made as wide as possible, i.e., 229–4219 (Table I). A material with

TABLE I
PCM MATERIALS USED FOR 16-CHANNEL OSELS

CH	Materials	McReynolds constant
1	OV-101	229
2	OV-3	423
3	OV-105	462
4	OV-7	592
5	OV-11	786
6	OV-17	884
7	OV-1701	789
8	OV-22	1075
9	OV-25	1175
10	OV-210	1520
11	OV-225	1813
12	OV-330	1671
13	SILAR-5CP	2428
14	SILAR-7CP	3200
15	SP-2340	3678
16	OV-275	4219

a larger McReynolds constant exhibits larger polarity. This, in turn, enables one to discriminate a wide range of odorants' polarities which are well known to be highly correlated with human perception [25]. In general, the higher polarity odorants adsorb more easily onto the OSEL with high polarity, and the lower polarity odorants adsorb more easily onto the OSEL with lower polarity. Second, for all the PCMs, the main chains of the compounds are selected to be siloxane because of their excellent stability against high temperatures. Thus, selected PCMs are listed in Table I. Carbon nanoparticles, for which a low-cost and mass-production compatible fabrication has been established, were adopted as electronic conduction sites within the PCMs.

C. Microheater

The temperature of all the 16 PCMs is controlled by a single heater consisting of a Pt-/Ti-wire patterned on a Si substrate [Fig. 2(a)]. Pt/Ti (200/10 nm) was vapor deposed on the Si substrate and patterned using photolithography to form a meander wiring. By driving the microheater by a constant current source with a pulsewidth modulation (PWM) scheme, a 0.8-W effective dc power output is obtained. Thus, one sensing cycle (desorption and adsorption) described in Fig. 3 is employed. The periods of heating and cooling are determined to allow the entire OSEL array to be heated (cooled) in a temperature range between 30 °C and 70 °C. The 16-channel PCM array was then, laminated on the microheater. The time constant (RC) calculated from the thermal resistance R (133.9 [K/W]) and thermal capacity C (0.4183 [J/K]) of the microheater is 56.0 [s], and the power of 0.8 W (voltage

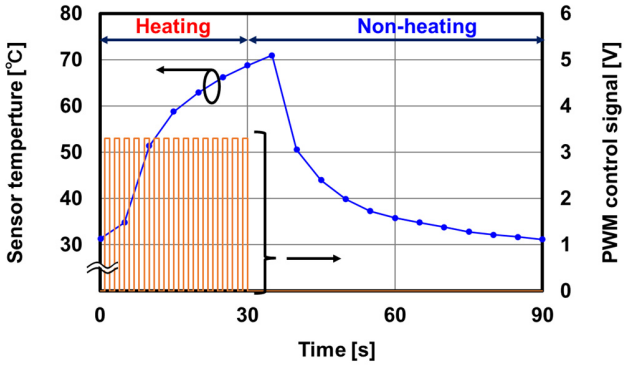

Fig. 3. Sensor temperature (blue line) and PWM signal (orange line) for one sensing cycle.

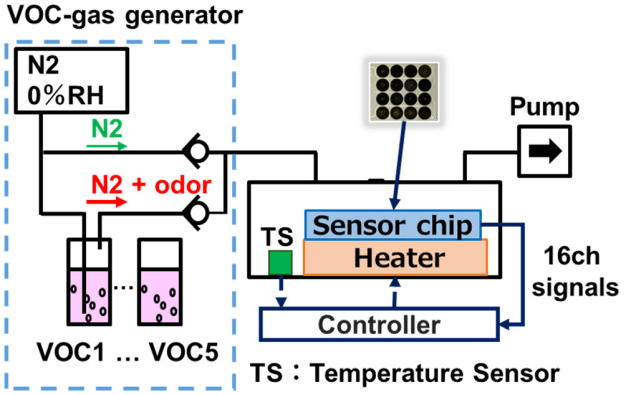

Fig. 4. Schematic of experimental setup consisting of a VOC-gas generator, TC-OSS, and a backside exhaustion pumping system.

16 [V], current 50 [mA]) is given to the heater. Under these conditions, the temperature can be raised to 70 °C by heating for 30 s. With this architecture, a total size of 6.5 mm (W) × 6.0 mm (D) × 1.05 mm (H), is realized.

III. RESULTS AND DISCUSSION

A. Experimental Setup

In Fig. 4, a schematic of the developed TC-OSS is illustrated. The TC-OSS is connected to a VOC-gas generator in front and to a pumping exhaustion line in the back. The VOC-gas generator consists of a concentration control part that generates a fixed concentration of a VOC by bubbling a VOC source with dry nitrogen gas and a humidity control part which generates a carrier gas, i.e., nitrogen with 0% relative humidity.

The flow rate of each gas is 50-mL/min set by the backside pump. As for odor sources, five kinds of VOCs and the dry nitrogen used in the standard qualification test of the olfactory measurement operator (in Japan) are prepared as listed in Table II [26]. The concentration of each VOC is set at the threshold of empirically determined human odor perception.

B. Characteristics of OSELs

1) Temperature Dependence of the Sensitivity Parameter: To determine the temperature control protocol, temperature dependence of the Sensitivity parameters [defined as (1)] are analyzed with all the VOCs listed in Table II. As an example, in Fig. 5, the temperature dependences (30 °C–80 °C) of Sen

TABLE II
STANDARD VOCS AS PREPARED ODOR SOURCES

Smell Label	Description	Gas Species	Concentration (ppm)
A	Flower	β-Phenylethyl alcohol	1.659
B	Sweet burnt	Methylcyclopentenolone	2.033
C	Socks	Isovaleric acid	4.749
D	Fruits	γ-Undecalactone	0.004
E	Musty	3-Methylindole	0.003

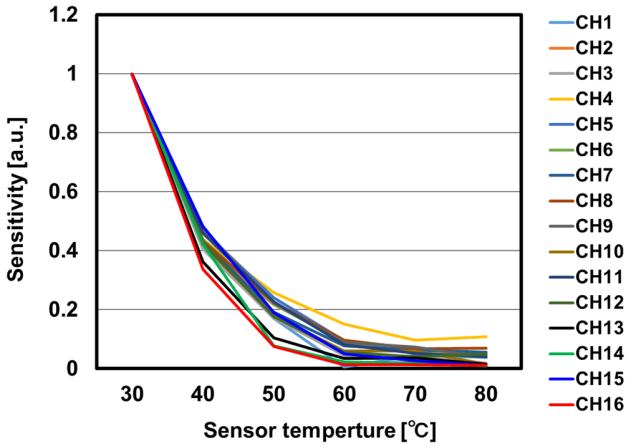

Fig. 5. Adsorption amount of odor molecules could be controlled by sensor temperature.

parameters of all 16 channels (OSELs) in response to the VOC of type A (1.659 ppm of β-Phenylethyl alcohol) are plotted. The Sen parameter of each channel is normalized by its value at a temperature of 30 °C. It is confirmed that Sen of all the OSELs indicating that the adsorption characteristics or odor sensing capabilities are nearly compatible among all the OSELs indicating that they are controllable with this unified temperature protocol. On the other hand, desorption of the decrease with nearly the same slope up to 40 °C (0.058 /°C), OSELs can be controlled by simply setting the reset temperature at 70 °C because Sen of all the OSELs reach 0.1 or below in a temperature range higher than ∼70 °C. Controllability and temperature uniformity with this architecture are demonstrated by the nearly identical response of all the PCMs (Fig. 5). Thus, we confirm that the developed 16 channels OSELs are controllable for both adsorption and desorption operations by the single microheater described in Section II-C.

2) Coverage of the Standard Odor Range: Next, we investigate the applicability of the developed TC-OSS to the standard odor range (Table II). In Fig. 6, output waveforms or the normalized resistance measured with a representative OSEL (channel 12) in response to five standards VOCs (Table II) and to dry nitrogen are plotted. We observe that for all five types of VOCs (even for types D and E with low concentrations), the OSEL output exhibits sizable variation indicating the applicability of the present OSEL to the wide odor range. Since the OSEL does not respond to nitrogen, the waveform of the

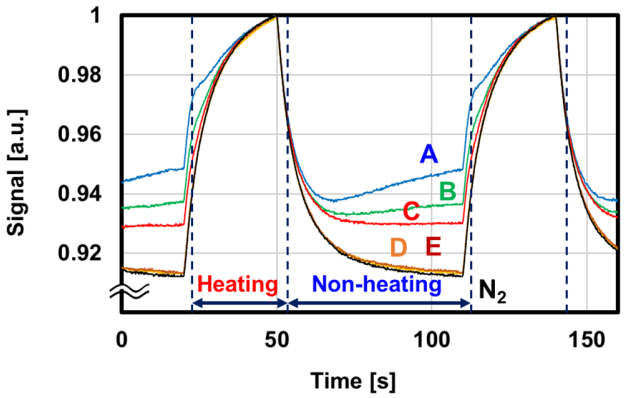

Fig. 6. Normalized signals output from channel 12 of OSEL in response to standard VOCs (Table II).

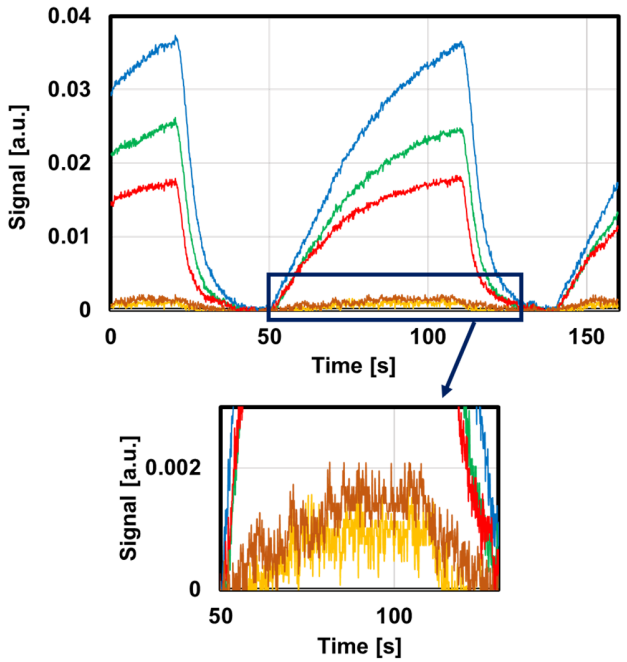

Fig. 7. Difference between odor and *N*2 waveforms (sensor CH12).

response to nitrogen (black line) shows the pure temperature characteristics of the OSEL itself. During the heating period, the microheater is turned on and the resistance increases with the rise of the sensor temperature. On the other hand, during the nonheating (cooling) period, the resistance decreases. It is noted that the time constants of the rising period (30 s) and falling period (60 s) are consistent with the estimation made in Section II-C.

To exclude the temperature dependence of the OSEL itself as described above, i.e., the response to the nitrogen flow, subtraction of the nitrogen signal is made from each signal with the VOC input and plotted in Fig. 7. Thus, the zero level of the vertical axis represents the output due only to nitrogen. Whereas the resistance value of the OSEL increases due to the adsorption of odor molecules in a lower temperature range (in the nonheating period) [1], [18], [19], the resistance value decreases (returning to the initial state) due to the desorption of the odor molecules from the PCM in a higher temperature range (during the heating period). These signals are considered to be due only to the VOCs. Taking the maximum values as

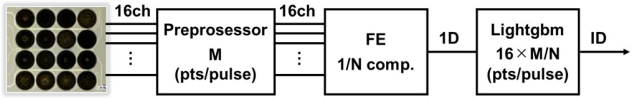

Fig. 8. Data flow for sensor signals. FE stands for FE producing 1-D vector data consisting of various feature parameters extracted from the raw input data with a compressibility, *N*. ID is identification data processed by Lightgbm. To Lightgbm, data of multiple cycles (typically 20) are fed.

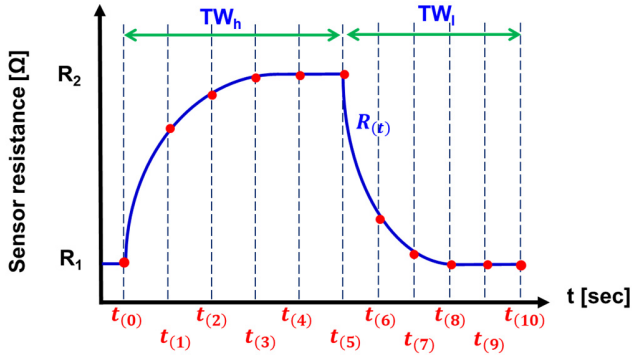

Fig. 9. How to divide waveforms when calculating features.

the signals and the variance of the signal fluctuations as noise, signals-to-noise (S/N) ratios for *A*–*C* are estimated to be 41.8, 37.4, and 36.4 dB, respectively. In the same way, even for the low-concentration samples of type D and E, S/N ratios of 14.6 and 16.2 dB, respectively, are obtained demonstrating the high sensitivity of the present OSELs.

C. VOCs Identification by a Machine Learning

A diagram of the data processing flow is illustrated in Fig. 8 describing the present system. Time-series data output from the 16 channels of OSELs are sampled with a 100-Hz sampling rate for 90 s leading to 9000 points/channel denoted as the output parameter of the preprocessor, M. Then, the data of each channel are fed into the feature extractor (FE) producing a 1-D $1 \times M/N$ vector data consisting of various feature parameters. Here, the parameter N represents an effective compressibility per channel. The feature parameters are sensitivity and slope [1], [27] of the raw data as listed in Table III. The sampling process of the typical sensor signal or resistance, $\boldsymbol{R}_{(t)}$, is illustrated in Fig. 9. Optimization of the compression ratio is determined experimentally. Finally, the 1-D vector data of the feature parameters are fed into a commonly used pattern recognizer, i.e., Lightgbm. Since adsorption speed and adsorption concentration are considered to different depending on the type of VOCs, the feature parameters are configured to detect these differences.

In actual experiments, we calculated the sensitivity parameters and slopes in a one cycle of the output signal waveform at ten predetermined timings giving 20 types of feature parameters, as illustrated in Fig. 9. Regarding to definition of the feature parameters in Table III, Sen(k) in (3) represents the rate of change of the signal from $t(0)$ (the measurement start point). SL(k) in (4) and (5) represents the slope of the interval from $t(k-1)$ to $t(k)$. $\mathrm{TW_h}$ is the time width of one heating cycle and $\mathrm{TW_l}$ is the nonheating cycle. Sen(k) represents the amount of response, and SL(k) represents the speed of response. These features are important factors for odor discrimination.

TABLE III
FEATURES LIST

feature	Formulas	
Sen (k) $k = 1\sim10$	$\frac{R_{(t(k))} - R_{(t(0))}}{R_{(t(0))}}$	(3)
SL (k) $k = 1\sim5$	$\frac{R_{(t(k))} - R_{(t(k-1))}}{TW_h/5}$	(4)
SL (k) $k = 6\sim10$	$\frac{R_{(t(k))} - R_{(t(k-1))}}{TW_l/5}$	(5)

TABLE IV
NUMBER OF DATA POINTS LIST

Parameter	Conventional	This work
Ch	16	16
M datapoints/cycle	9000	9000
N compressibility	1	450
Total (= CH x M / N)	144,000	320

In the present work, compressibility N is 450 (9000 points/20 feature values). A total of 320 [16(ch) × 9000(M)/450(N)] feature parameters are obtained as described at the bottom of the right column of Table IV. Even with this highly compressed data, pattern recognition by Lightgbm is shown to be possible by the proper configuration of a decision tree. It is noted that in the reference system, the raw data are directly input to the Lightgbm system as a huge set of explanatory variables, i.e., 144 000 points/cycle, as described in the bottom of the left column in Table IV. Pattern discrimination using such a large amount of data is impractical, particularly for the present real-time processing system.

The data sets of 200 pulses (40 pulses × 5 standard VOCs), and the 320 types of the feature values were calculated from all response pulses of the standard VOCs. As an example, Fig. 10(a) shows the response (40 pulses × 5 standard VOCs) of a sensitivity parameter, described as SL(10), of CH 12 to the five standard VOCs (Table II). In this case, while the difference among *A*–*C* is clearly recognized, the difference between *D* and *E* is not well resolved. However, by utilizing the response of Sen(10) of CH14, not only the difference among *A*–*C* but also the difference between *D* and *E* is clearly

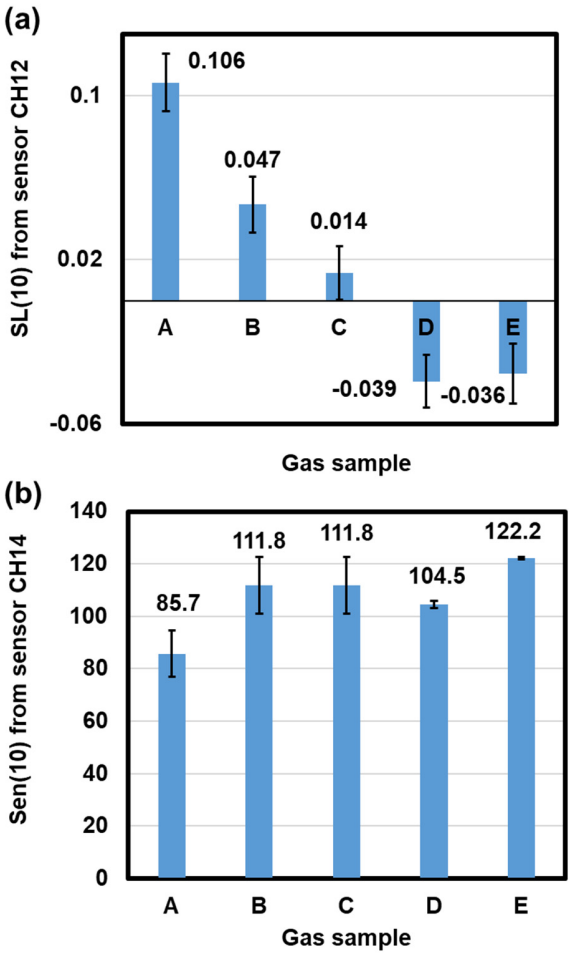

Fig. 10. Response of (a) SL(10) from sensor CH12 and (b) SN(10) from sensor CH14.

TABLE V
RESULT OF THE PREDICTION OF THE CLASSIFICATION USING LIGHTGBM

Accuracy 95.8±2.7%		Predicted label					F score
		A	B	C	D	E	
True label	A	19	1	0	0	0	0.97
	B	0	20	0	0	0	0.98
	C	0	0	20	0	0	1.0
	D	0	0	0	19	1	0.86
	E	0	0	0	5	15	0.83

distinguished, demonstrating the effectiveness of the present methodology.

Finally, machine learning is performed using all 320 types of feature values as input data to classify standard VOCs. Lightgbm [28], a data analysis method termed as "supervised learning," is used as the machine learning algorithm. It is based on a decision tree method classifying target variables (types of VOCs) at each node by utilizing the feature values

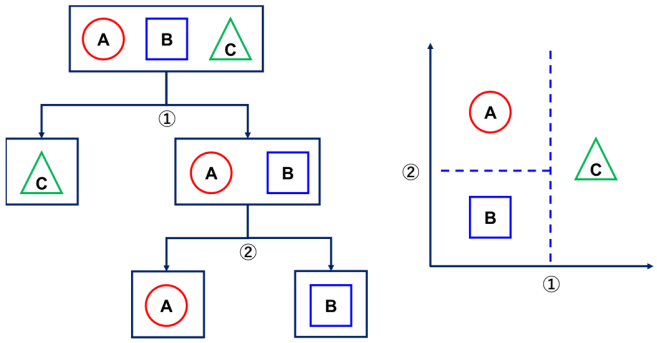

Fig. 11. Lightgbm, one of the decision tree methods.

as explanatory variables (Fig. 11). All data were divided into two sets, used as training data and evaluation data. The data combination was randomly changed, and 100 repeated evaluations were performed. As shown in Table V, we succeeded in predicting five standard VOCs with a high accuracy rate of 95.8% ± 2.7%. As shown in Table II, the concentrations of D and E are only about 1/1000 of those of A–C. Detecting D and E is very difficult, but the present OSS successfully detects them with the F-score as high as 0.86 and 0.83, respectively. The F-score represents the harmonic mean of precision and recall as follows [29]:

$$F\ \text{score} = 2 \cdot \frac{\text{Precision} \cdot \text{Recall}}{\text{Precision} + \text{Recall}}. \tag{6}$$

IV. CONCLUSION

1) We demonstrated a compact and highly sensitive TC-OSS comprising 16 PCMs with high heat resistance and a microheater.
2) By employing the single heater control architecture, the compactness of the system due to the elimination of a significant amount of gas flow-control parts necessary for conventional systems is demonstrated.
3) We confirmed the high sensitivity for five standard VOCs (Table II) such that the SNR of the detected signals is as high as ∼15 dB even with the VOC level of 3 ppb.
4) With the assistance of a Lightgbm AI system, we succeeded in predicting the VOCs with a high accuracy rate of 95.8% ± 2.7% (Table V).
5) The developed TC-OSS is expected to be highly useful for many social infrastructures.

REFERENCES

[1] R. Yatabe et al., "Odor sensor system using chemosensitive resistor array and machine learning," *IEEE Sensors J.*, vol. 21, no. 2, pp. 2077–2083, Jan. 2021.
[2] A. Hannon, Y. Lu, J. Li, and M. Meyyappan, "A sensor array for the detection and discrimination of methane and other environmental pollutant gases," *Sensors*, vol. 16, no. 8, p. 1163, Jul. 2016.
[3] A. D'Amico et al., "An investigation on electronic nose diagnosis of lung cancer," *Lung Cancer*, vol. 68, no. 2, pp. 170–176, May 2010.
[4] A. D. A. D. Wilson, "Recent progress in the design and clinical development of electronic-nose technologies," *Nanobiosensors Disease Diagnosis*, vol. 2016, no. 5, pp. 15–27, Jan. 2016.
[5] P. Kanakam, S. M. Hussain, and A. Chakravarthy, "Cogno-detective system for body odor sensing," in *Proc. IEEE Int. Conf. Comput. Intell. Comput. Res. (ICCIC)*, Dec. 2017, pp. 1–3.

[6] P. Kanakam, S. M. Hussain, and A. S. N. Chakravarthy, "Electronic noses: Forestalling fire disasters: A technique to prevent false fire alarms and fatal casualties," in *Proc. IEEE Int. Conf. Comput. Intell. Comput. Res. (ICCIC)*, Madurai, India, Dec. 2015, pp. 1–6, doi: 10.1109/ICCIC.2015.7435629.

[7] N. R. Mavani, J. M. Ali, S. Othman, M. A. Hussain, H. Hashim, and N. A. Rahman, "Application of artificial intelligence in food industry—A guideline," *Food Eng. Rev.*, vol. 14, no. 1, pp. 134–175, Mar. 2022.

[8] S. Firestein, "How the olfactory system makes sense of scents," *Nature*, vol. 413, no. 6852, pp. 211–218, Sep. 2001.

[9] M. Conover, *Predator-Prey Dynamics: The Role of Olfaction*. Boca Raton, FL, USA: CRC Press, 2007, p. 39.

[10] J. W. Gardner and P. N. Bartlett, "A brief history of electronic noses," *Sens. Actuators B, Chem.*, vol. 18, nos. 1–3, pp. 210–211, Mar. 1994.

[11] K. Persaud and G. Dodd, "Analysis of discrimination mechanisms in the mammalian olfactory system using a model nose," *Nature*, vol. 299, no. 5881, pp. 352–355, Sep. 1982.

[12] H. T. Nagle, R. Gutierrez-Osuna, and S. S. Schiffman, "The how and why of electronic noses," *IEEE Spectr.*, vol. 35, no. 9, pp. 22–31, Sep. 1998.

[13] M. Zarzo and D. T. Stanton, "Identification of latent variables in a semantic odor profile database using principal component analysis," *Chem. Senses*, vol. 31, no. 8, pp. 713–724, Oct. 2006.

[14] P. C. Jurs, G. A. Bakken, and H. E. McClelland, "Computational methods for the analysis of chemical sensor array data from volatile analytes," *Chem. Rev.*, vol. 100, no. 7, pp. 2649–2678, Jul. 2000.

[15] I. Lundström, S. Shivaraman, C. Svensson, and L. Lundkvist, "A hydrogen-sensitive MOS field-effect transistor," *Appl. Phys. Lett.*, vol. 26, no. 2, pp. 55–57, Jan. 1975.

[16] T. Nakamoto, A. Fukuda, and T. Moriizumi, "Perfume and flavour identification by odour-sensing system using quartz-resonator sensor array and neural-network pattern recognition," *Sens. Actuators B, Chem.*, vol. 10, no. 2, pp. 85–90, Jan. 1993.

[17] S.-M. Chang, E. Tamiya, I. Karube, M. Sato, and Y. Masuda, "Odorant sensor using lipid-coated SAW resonator oscillator," *Sens. Actuators B, Chem.*, vol. 5, nos. 1–4, pp. 53–58, Aug. 1991.

[18] B. Wyszynski et al., "Array of chemosensitive resistors with composites of gas chromatography (GC) materials and carbon black for detection and recognition of VOCs: A basic study," *Sensors*, vol. 17, no. 7, p. 1606, Jul. 2017.

[19] A. Shunori et al., "Multichannel odor sensor system using chemosensitive resistors and machine learning," in *Proc. IEEE Int. Symp. Olfaction Electron. Nose (ISOEN)*, Fukuoka, Japan, May 2019, pp. 1–3.

[20] J. Burgués, M. D. Esclapez, S. Doñate, L. Pastor, and S. Marco, "Aerial mapping of odorous gases in a wastewater treatment plant using a small drone," *Remote Sens.*, vol. 13, no. 9, p. 1757, Apr. 2021.

[21] M. Abdelkhalek, S. Alfayad, F. Benouezdou, M. B. Fayek, and L. Chassagne, "Compact and embedded electronic nose for volatile and non-volatile odor classification for robot applications," *IEEE Access*, vol. 7, pp. 98267–98276, 2019.

[22] J. Laothawornkitkul et al., "Discrimination of plant volatile signatures by an electronic nose: A potential technology for plant pest and disease monitoring," *Environ. Sci. Technol.*, vol. 42, no. 22, pp. 8433–8439, Nov. 2008.

[23] T. Zarra, V. Naddeo, and V. Belgiorno, "A novel tool for estimating the odour emissions of composting plants in air pollution management," *Global Nest J.*, vol. 11, no. 4, pp. 477–486, 2009.

[24] W. O. McReynolds, "Gas chromatographic retention data," *J. Chromatograph. Sci.*, vol. 8, no. 8, pp. 685–691, 1970.

[25] G. A. Bell, D. G. Laing, and H. Panhuber, "Odour mixture suppression: Evidence for a peripheral mechanism in human and rat," *Brain Res.*, vol. 426, no. 1, pp. 8–18, Nov. 1987.

[26] T. Miwa et al., "Clinical practice guidelines for the management of olfactory dysfunction—Secondary publication," *Auris Nasus Larynx*, vol. 46, no. 5, pp. 653–662, Oct. 2019.

[27] J. Yan et al., "Electronic nose feature extraction methods: A review," *Sensors*, vol. 15, no. 11, pp. 27804–27831, Nov. 2015.

[28] K. Guolin et al., "LightGBM: A highly efficient gradient boosting decision tree," in *Proc. Adv. Neural Inf. Process. Syst.*, 2017, pp. 1–9.

[29] T. Saito and M. Rehmsmeier, "The precision-recall plot is more informative than the ROC plot when evaluating binary classifiers on imbalanced datasets," *PLoS One*, vol. 10, no. 3, Mar. 2015, Art. no. e0118432.

Toshiki Niinomi received the M.S. degree in quantum engineering from Nagoya University, Nagoya, Japan, in 2018.

He joined Panasonic Corporation, Osaka, Japan, in 2018. He is currently a Staff Engineer with Panasonic Industry Corporation, Osaka.

Atsuo Nakao received the M.S. degree in materials engineering from Kyoto University, Kyoto, Japan, in 2008.

He joined Panasonic Electronic Devices Company Ltd., Osaka, japan, in 2008. He is currently a Chief Engineer with Panasonic Industry Corporation, Osaka, Japan.

Yosuke Hanai received the master's degree in agriculture from Mie University, Tsu, Japan, in 2005, and the Ph.D. degree in agriculture from Kyoto University, Kyoto, Japan, in 2014.

From 2010 to 2013, he worked at the Engineering Department, Nagoya University, Nagoya, Japan. He moved to the Engineering Division, Panasonic AIS Corporation, Osaka, in 2013. He has been a Staff Engineer with Panasonic Corporation, Osaka, Japan, since 2019. He is currently a Staff Engineer with Panasonic Industry Corporation, Osaka.

Hiroshi Ushio received the M.S. degree in electrical and electronics engineering from the Himeji Institute of Technology, Hyogo, Japan, in 2003.

He joined Panasonic Electronic Devices Company Ltd., in 2003. He is currently a Staff Engineer with Panasonic Industry Corporation, Osaka, Japan.

Takuya Hayashi received the M.S. degree in electrical and electronics from the Tokyo University of Agriculture and Technology, Tokyo, Japan, in 2003.

He joined Panasonic Electronic Devices Company Ltd., in 2003. He is currently a Staff Engineer with Panasonic Industry Corporation, Osaka, Japan.

Masaya Nakatani received the bachelor's degree in physics from the University of Tsukuba, Tsukuba, Japan, in 1989.

He joined Panasonic Corporation, Osaka, Japan, in 1989. He is currently a Chief Engineer with Panasonic Industry Corporation, Osaka. He is managing the Research and Development Team for Bio Sensor.